

# Experiments For CP-Violation: A Giant Liquid Argon Scintillation, Cerenkov And Charge Imaging Experiment ?<sup>a</sup>

A. Rubbia<sup>b</sup>

Institut für Teilchenphysik, ETHZ, CH-8093 Zürich, Switzerland

## Abstract

In this paper we address a class of “ultimate” generation experiments for the search of CP-violation in neutrino oscillations. Neutrino factories require large magnetized detectors. New generation superbeams or beta-beams need giant detectors. The liquid Argon TPC technology has great potentials for both applications. Although the ICARUS program has demonstrated that this technology is mature, the possibility to built a giant liquid argon TPC is viewed by many as a technically impossible and unsafe task. We argue that a giant liquid argon Cerenkov and charge Imaging experiment would be an ideal match for a superbeam or a betabeam. Such a detector would in addition cover a broad physics program, including the observation of atmospheric neutrinos, solar neutrinos, supernova neutrinos, and search for proton decays, in addition to the accelerator physics program. We show a potential implementation of such a giant LAr detector and argue that it could be technically feasible. The possibility to host such a detector in an underground cavern is under study.

---

<sup>a</sup>Invited talk at the II International Workshop on: NEUTRINO OSCILLATIONS IN VENICE, Venice (Italy), December 2003.

<sup>b</sup>Andre.Rubbia@cern.ch

# 1 Introduction

How can one experimentally observe the CP-violation in the leptonic sector? From the unitary mixing matrix, which can be parameterized as

$$U(\theta_{12}, \theta_{13}, \theta_{23}, \delta) = \begin{pmatrix} c_{12}c_{13} & s_{12}c_{13} & s_{13}e^{-i\delta} \\ -s_{12}c_{23} - c_{12}s_{13}s_{23}e^{i\delta} & c_{12}c_{23} - s_{12}s_{13}s_{23}e^{i\delta} & c_{13}s_{23} \\ s_{12}s_{23} - c_{12}s_{13}c_{23}e^{i\delta} & -c_{12}s_{23} - s_{12}s_{13}c_{23}e^{i\delta} & c_{13}c_{23} \end{pmatrix} \quad (1)$$

with  $s_{ij} = \sin \theta_{ij}$  and  $c_{ij} = \cos \theta_{ij}$ , we get the freedom of the complex phase (physical only if  $\theta_{13} \neq 0$ !). We know that

1. the  $\delta$ -phase can only be observed in an appearance experiment since the disappearance is a T-symmetric process;
2. the effect for antineutrinos should be opposite to neutrinos ( $\delta \rightarrow -\delta$ );
3. it should have the expected  $L/E_\nu$  dependence, where  $E_\nu$  is the neutrino energy;

Considering oscillations involving electron and muon flavors, the oscillation probability, in the parameterization described above, is:

$$\begin{aligned} P(\nu_e \rightarrow \nu_\mu) &= P(\bar{\nu}_\mu \rightarrow \bar{\nu}_e) = \\ 4c_{13}^2 &\left[ \sin^2 \Delta_{23} s_{12}^2 s_{13}^2 s_{23}^2 + c_{12}^2 (\sin^2 \Delta_{13} s_{13}^2 s_{23}^2 + \sin^2 \Delta_{12} s_{12}^2 (1 - (1 + s_{13}^2) s_{23}^2)) \right] \\ &- \frac{1}{2} c_{13}^2 \sin(2\theta_{12}) s_{13} \sin(2\theta_{23}) \cos \delta [\cos 2\Delta_{13} - \cos 2\Delta_{23} - 2 \cos(2\theta_{12}) \sin^2 \Delta_{12}] \\ &+ \frac{1}{2} c_{13}^2 \sin \delta \sin(2\theta_{12}) s_{13} \sin(2\theta_{23}) [\sin 2\Delta_{12} - \sin 2\Delta_{13} + \sin 2\Delta_{23}] \quad (2) \end{aligned}$$

where  $\Delta_{jk} \equiv \Delta m_{jk}^2 L / 4E_\nu$  (in natural units).

We note that a precise measurement of the  $\nu_e \rightarrow \nu_\mu$  oscillation probability can yield information of the  $\delta$ -phase provided that the other oscillation parameters in the expression are known sufficiently accurately. In practice, one can introduce a certain number of discriminants[1, 2] which are good quantities to experimentally search for a non-vanishing phase:

1.  $\Delta_\delta \equiv P(\nu_e \rightarrow \nu_\mu, \delta = +\pi/2) - P(\nu_e \rightarrow \nu_\mu, \delta = 0)$

The discriminant  $\Delta_\delta$  can be used in an experiment where one is comparing the measured  $\nu_e \rightarrow \nu_\mu$  oscillation probability as a function of the neutrino energy  $E_\nu$  with a ‘‘Monte-Carlo prediction’’ of the spectrum in absence of  $\delta$ -phase.

2.  $\Delta_{CP}(\delta) \equiv P(\nu_e \rightarrow \nu_\mu, \delta) - P(\bar{\nu}_e \rightarrow \bar{\nu}_\mu, \delta)$

The discriminant  $\Delta_{CP}$  can be used in an experiment by comparing the appearance of negative and positive muons as a function of the neutrino energy  $E_\nu$  for  $\nu_e$  and  $\bar{\nu}_e$  sources.

3.  $\Delta_T(\delta) \equiv P(\nu_e \rightarrow \nu_\mu, \delta) - P(\nu_\mu \rightarrow \nu_e, \delta)$  or  $\bar{\Delta}_T(\delta) \equiv P(\bar{\nu}_e \rightarrow \bar{\nu}_\mu, \delta) - P(\bar{\nu}_\mu \rightarrow \bar{\nu}_e, \delta)$

The discriminant  $\Delta_T$  can be used in an experiment by comparing the appearance of  $\nu_\mu$  **and**  $\nu_e$  (resp.  $\bar{\nu}_\mu$  **and**  $\bar{\nu}_e$ ) as a function of the neutrino energy  $E_\nu$ .

Each of these discriminants have their advantages and disadvantages[1]. The  $\Delta\delta$ -method can provide excellent determination of the phase limited only by the statistics of accumulated events, in practice, systematic effects will have to be carefully kept under control in order to look for a small effect in a seen-data versus Monte-Carlo-expected comparison. In addition, the precise knowledge of the other oscillation parameters will be important. The  $\Delta_{CP}$  is quite straight-forward, it suffers, however, from matter effects which “spoil”  $\Delta_{CP}$  since it involves both neutrinos and antineutrinos, which oscillate differently through matter. Hence, the  $\Delta_{CP}$  requires a good understanding of the effects related to matter. These effects increase with baseline and are maximum around the “resonance energy” around  $E_\nu \simeq 10 \text{ GeV}$ [1]. The  $\Delta_T$  is the theoretically cleanest method, since it does not suffer from the problems of  $\Delta\delta$  and  $\Delta_{CP}$ . Indeed, a difference in oscillation probabilities between  $\nu_e \rightarrow \nu_\mu$  and  $\nu_\mu \rightarrow \nu_e$  would be a direct proof for a non-vanishing  $\delta$ -phase. In addition, matter affects both probabilities in a same way, since it involves only neutrinos (resp. antineutrinos for  $\bar{\Delta}_T$ ).

## 2 Guidelines for a CP-violation neutrino oscillation experiment

A long-baseline neutrino oscillation experiment designed to search for a non-vanishing  $\delta$ -phase is necessarily an “ultimate” (or at least a “phase-II”) experiment since it should

- be designed to have ample statistics (for a given  $\theta_{13}$ ) to precisely determine the oscillation probability as a function of the neutrino energy; hence its size will depend on the actual value of  $\theta_{13}$  (and if  $\theta_{13} > 0$  !)
- have an excellent energy resolution to observe the energy dependence of the oscillation probability and help lift degeneracy of the parameters governing the neutrino oscillations (see e.g. Ref.[1]);
- be performed at a wide-band neutrino beam to cover enough “oscillations” peaks or do “counting” at different neutrino beam energy settings;
- have the possibility to study neutrinos and antineutrinos ideally separately in order to lift degeneracies (even in the counting mode).

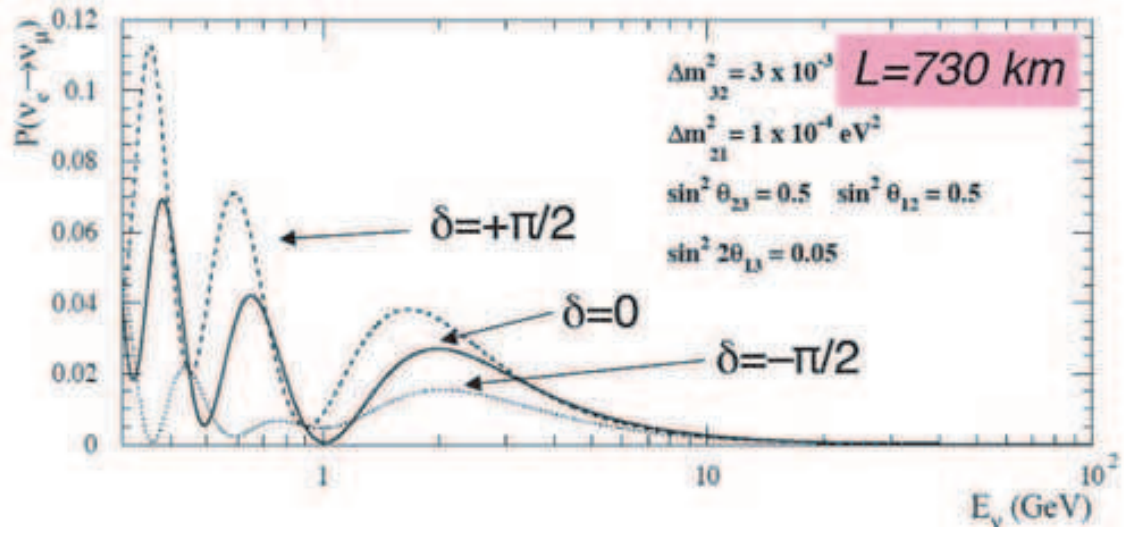


Figure 1: The  $\nu_\mu \rightarrow \nu_e$  oscillation probability as a function of neutrino energy for different values of the  $\delta$  phase for a given set of oscillation parameters and a distance of 730 km.

Figure 1 illustrates qualitatively the fact that a measurement of the oscillation probability *as a function of energy with good resolution* would indeed provide direct information on the  $\delta$ -phase, since this latter introduces a well-defined energy dependence of the oscillation probability, which is different from the, say, energy dependence introduced by  $\theta_{13}$  alone (when  $\delta = 0$ ).

To study these oscillations, one considers three types of neutrino beams produced at accelerators:

- Superbeams: these are conventional pion beams of high intensity, where the sign of the focusing can be selected to enhance neutrinos or antineutrinos components

$$\pi^+ \rightarrow \mu^+ + \nu_\mu \quad \text{or} \quad \pi^- \rightarrow \mu^- + \bar{\nu}_\mu \quad (3)$$

- Betabeams[3]: these are radioactive storage rings, where the type of ion can be chosen to select electron-neutrinos or electron-antineutrinos

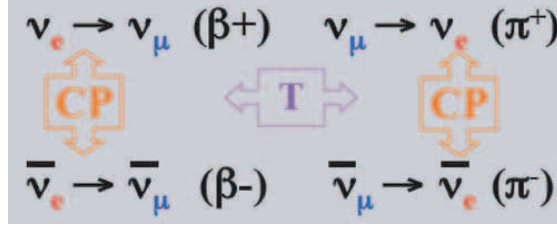
$${}^Z A \rightarrow {}^{Z-1} A \beta^+ \nu_e \quad \text{or} \quad {}^Z A \rightarrow {}^{Z+1} A \beta^- \bar{\nu}_e \quad (4)$$

- Neutrino factories[4]: these are muon storage rings, where the charge of the muons can be a priori chosen to select neutrinos/antineutrinos of given flavors-pairs

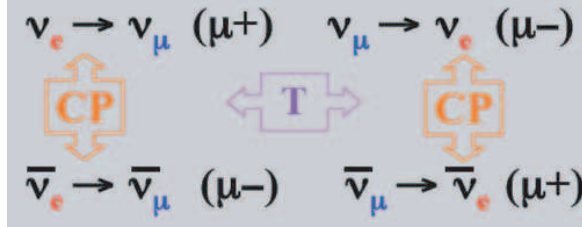
$$\mu^- \rightarrow e^- \bar{\nu}_e \nu_\mu \quad \text{or} \quad \mu^+ \rightarrow e^+ \nu_e \bar{\nu}_\mu \quad (5)$$

From the point of view of neutrino oscillation studies, these beams turn out to be very complementary. Indeed, the combination of superbeams ( $\pi^\pm$ ) and

beta-beams ( $\beta^\pm$ ) allows to study CP- and T-violation by a direct comparison of the results from the various sources:



In a similar way, a neutrino factory ( $\mu^\pm$ ) can provide all possible combinations to access directly CP- and T-violation:



However, it goes without saying that these types of beams require very different accelerator technologies. Also from a detector point of view, there are quite distinct optimizations required for super- and beta-beams on one side and neutrino factory on the other, as discussed in the following sections. In particular, *detectors for a neutrino factory are necessarily magnetized, hence this will limit their size to say 10-50 kton, while detectors for super- and beta-beams are conceived as giant non-magnetized experiments with sizes of say 100-1000 kton.*

## 2.1 Detectors for the super and beta-beams

Superbeams and betabeams are typically designed with energies in the range of the GeV or below. Since the cross-sections are approximately linear with energy, detectors must be very massive, typically in the range of 100-1000 kton. For the superbeams, a good  $e/\pi^0$  discrimination is important in order to suppress the neutral current background with a leading  $\pi^0$ :

$$\nu N \rightarrow \pi^0 + X \quad (6)$$

from the oscillation channel

$$\nu_\mu \rightarrow \nu_e \quad \text{and} \quad \nu_e N \rightarrow e + X \quad (7)$$

In the case of the betabeams, a good  $\mu/\pi^\pm$  discrimination is important in order to suppress the neutral current background with a charged leading  $\pi^\pm$ :

$$\nu N \rightarrow \pi^\pm + X \quad (8)$$

from the oscillation channel

$$\nu_e \rightarrow \nu_\mu \quad \text{and} \quad \nu_\mu N \rightarrow \mu + X \quad (9)$$

For the beta-beam there is a minimum baseline  $L_{min}$  between the source and the detector. Indeed, the oscillation is detected through the muon appearance channel which has an energy threshold of about 110 MeV. Hence,

$$L_{min} = \pi \frac{110 \text{ MeV}}{1.27 \Delta m^2} \approx 136 \text{ km} \quad (10)$$

for  $\Delta m^2 = 2 \times 10^{-3} \text{ eV}^2$ .

Summarizing, the *ideal detector at the superbeam or beta-beam should possess the following characteristics:*

- **Low energy threshold:** the detector should be able to detect, reconstruct and analyse events with neutrino energies in the GeV and below.
- **Particle identification:** the detector should be able to identify and measure electrons and muons, and separate them from other hadrons (typ. neutral and charged pions).
- **Energy resolution:** the incoming neutrino energy  $E_\nu$  is reconstructed as  $E_\nu = E_\ell + E_{had}$ , where  $E_\ell$  is the leading lepton energy and  $E_{had}$  is the hadronic energy. Hence, detector with better energy resolution will reconstruct the parameter of the incoming neutrino better, and therefore the oscillation probability<sup>a</sup>.
- **Isotropy:** at low energy final state particles are produced at all angle, in particular, the leading lepton can even be produced backward. This is increased on a nuclear target by the Fermi motion. The probably most efficient way to detect these particles is to build a large neutrino detector, *isotropic in nature*, capable of measuring equally well particles at all angles. This is also a necessary condition for studying astrophysical sources and look for proton decay.

We note that a magnetic field is not necessarily mandatory for these experiments.

## 2.2 Detectors for the neutrino factory

Neutrino factories are typically designed with energies much higher than the GeV. Given energies in the range of 10 GeV, detectors are typically in the range

---

<sup>a</sup>Note that it is often said that Fermi motion spoils energy resolution at low energy. This is not true when the final state is measured completely. Fermi motion can introduce a high momentum imbalance (up to 200 MeV), however, the energy available is related to the binding energy in the nucleus and is hence small compared to the incoming neutrino energy.

of 10-50 kton. At high energy, one could independently study the following flavor transitions:

$$\mu^- \rightarrow e^- \quad \bar{\nu}_e \quad \nu_\mu$$

$$\rightarrow \nu_e \rightarrow e^- \text{ appearance} \quad (11)$$

$$\rightarrow \nu_\mu \text{ disappearance, same sign muons} \quad (12)$$

$$\rightarrow \nu_\tau \rightarrow \tau^- \text{ appearance, high energy nu's} \quad (13)$$

$$\rightarrow \bar{\nu}_e \text{ disappearance} \quad (14)$$

$$\rightarrow \bar{\nu}_\mu \rightarrow \mu^+ \text{ appearance, wrong sign muons} \quad (15)$$

$$\rightarrow \bar{\nu}_\tau \rightarrow \tau^+ \text{ appearance, high energy nu's} \quad (16)$$

plus 6 other charge conjugate processes initiated from  $\mu^+$  decays. *The ideal neutrino detector should be able to measure these 12 different processes as a function of the baseline  $L$  and of the neutrino energy  $E_\nu$ !*

Of particular interest are the charged current neutrino interactions, since they can in principle be used to tag the neutrino flavor and helicity, through the detection and identification of the final state charged lepton:

$$\nu_\ell N \rightarrow \ell^- + \text{hadrons} \quad \bar{\nu}_\ell N \rightarrow \ell^+ + \text{hadrons} \quad (17)$$

Hence, the *ideal detector at the neutrino factory should possess the following characteristics:*

- **Particle identification:** the detector should be able to identify and measure the leading charged lepton of the interaction, in order to tag the incoming neutrino flavor.
- **Charge identification:** the sign of the leading lepton charge should be measured, since it tags the helicity of the incoming neutrino. The detector must necessarily be magnetized.
- **Energy resolution:** the incoming neutrino energy  $E_\nu$  is reconstructed as  $E_\nu = E_\ell + E_{had}$ , where  $E_\ell$  is the leading lepton energy and  $E_{had}$  is the hadronic energy. Hence, detector with better energy resolution will reconstruct the parameter of the incoming neutrino better, and therefore the oscillation probability.
- **Isotropy:** one might want to perform various similar experiments at different baselines. The probably most efficient way to achieve this is to build a large neutrino detector, *isotropic in nature*, capable of measuring equally well neutrinos from different sources located at different baselines  $L$ . Because of the spherical shape of the Earth, sources located at different baselines  $L$  will reach the detector “from below” at different angles. Isotropy of reconstruction is also a necessary condition for studying astrophysical sources and look for proton decay.

### 3 The liquid Argon Technology

The technology of the Liquid Argon Time Projection Chamber (LAr TPC), first proposed by C. Rubbia in 1977 [5], was conceived as a tool for a completely uniform imaging with high accuracy of massive volumes. The operational principle of the LAr TPC is based on the fact that in highly purified LAr ionization tracks can be transported practically undistorted by a uniform electric field over macroscopic distances. Imaging is provided by a suitable set of electrodes (wires) placed at the end of the drift path continuously sensing and recording the signals induced by the drifting electrons.

Non-destructive read-out of ionization electrons by charge induction allows to detect the signal of electrons crossing subsequent wire planes with different orientation. This provides several projective views of the same event, hence allowing space point reconstruction and precise calorimetric measurement.

The main technological challenges of this detection technique have been recently summarized elsewhere[6]. They mainly consisted in: (1) techniques of Argon purification (2) operation of wire chambers in cryogenic liquid and without charge amplification (3) extremely low-noise analog electronics (4) continuous wave-form recording and digital signal processing.

The feasibility of the technology has been demonstrated by the extensive ICARUS R&D programme, which included ten years of studies on small LAr volumes (proof of principle, LAr purification methods, read-out schemes, electronics) and five years of studies with several prototypes of increasing mass (purification technology, collection of physics events, pattern recognition, long duration tests, read-out technology). The largest of these devices had a mass of 3 tons of LAr [7, 8] and has been operated continuously for more than four years, collecting a large sample of cosmic-ray and gamma-source events. Furthermore, a smaller device (50 l of LAr [9]) was exposed to the CERN neutrino beam, demonstrating the high recognition capability of the technique for neutrino interaction events.

The realization of the T600 detector (from design to construction) lasted about four years and culminated with a full test of the experimental set-up, carried out at surface during 2001. This test demonstrated the maturity of the project. All technical aspects of the system, namely cryogenics, LAr purification, read-out chambers, detection of LAr scintillation light, electronics and DAQ had been tested and performed as expected. Statistically significant samples of cosmic-ray events (long muon tracks, hadronic interactions (see e.g Figure 2), spectacular high-multiplicity muon bundles, electromagnetic and hadronic showers, low energy events) were recorded. The analysis of these events has allowed the development and fine tuning of the off-line tools for the event reconstruction and the extraction of physical quantities. It has also demonstrated the performance of the detector in a quantitative way.



Figure 2: Hadronic interaction collected during the ICARUS T600 technical run on the surface.

The detector performance can be summarized as:

- a tracking device with precise event topology reconstruction
- momentum estimation via multiple scattering
- measurement of local energy deposition ( $dE/dx$ ), providing  $e/\pi^0$  separation (sampling typ.  $2\%X_0$ ), particle identification via range versus  $dE/dx$  measurement
- total energy reconstruction of the event from charge integration (the volume can be considered as a full-sampling, fully homogenous calorimeter) providing excellent accuracy for contained events

The energy resolutions are:

- $\sigma/E = 11\%/\sqrt{E(MeV)} \oplus 2\%$  for low energy electrons (measured[10])
- $\sigma/E \approx 3\%/\sqrt{E(GeV)}$  for electromagnetic showers
- $\sigma/E \approx 30\%/\sqrt{E(GeV)}$  for hadronic showers (pure LAr)
- $\sigma/E \approx 17\%/\sqrt{E(GeV)}$  for hadronic showers (TMG doped LAr)

It is fair to say that the technique has reached a high level of maturity.

## 4 A magnetized Liquid Argon TPC

Liquid argon imaging provides very good tracking with  $dE/dx$  measurement, and excellent calorimetric performance for contained showers. This allows for

a very precise determination of the energy of the particles in an event. This is particularly true for electron showers, which energy is very precisely measured.



Figure 3: Magnetized liquid argon TPC: simulation of the 2.5 GeV electron shower in liquid argon. The field has a strength  $B=1$  T and is directed perpendicular to the sheet-plane.

The possibility to complement these features with those provided by a magnetic field has been considered[2] and would open new possibilities:

- charge discrimination
- momentum measurement of particles escaping the detector (e.g. high energy muons)
- very precise kinematics, since the measurements are multiple scattering dominated (e.g.  $\Delta p/p \simeq 4\%$  for a track length of  $L = 12$  m and a field of  $B = 1T$ ).

The orientation of the magnetic field is such that the bending direction is in the direction of the drift where the best spatial resolution is achieved (e.g. in the ICARUS T600 a point resolution of  $400 \mu m$  was obtained). The magnetic field is hence perpendicular to the electric field. The Lorentz angle is expected to be very small in liquid (e.g.  $\approx 30 mrad$  at  $E = 500$  V/cm and  $B = 0.5T$ ). Embedding the volume of argon into a magnetic field would therefore not alter the imaging properties of the detector and the measurement of the bending of charged hadrons or penetrating muons would allow a precise determination of the momentum and a determination of their charge.

The required magnetic field for charge discrimination for a path  $x$  in the liquid Argon is given by the bending

$$b \approx \frac{l^2}{2R} = \frac{0.3B(T)(x(m))^2}{2p(GeV)} \quad (18)$$

and the multiple scattering contribution:

$$MS \approx \frac{0.02(x(m))^{3/2}}{p(GeV)} \quad (19)$$



Figure 4: Magnetized liquid argon TPC: ongoing R&D to test liquid argon imaging in a magnetic field. (left) CAD drawing of the chamber; the direction of the fields and a bending track is shown (right) actual setup.

The requirement for a  $3\sigma$  charge discrimination can be written as:  $b^+ - b^- = 2b > 3MS$ , which implies:

$$B \geq \frac{0.2(T)}{\sqrt{x(m)}} \quad (20)$$

For long penetrating tracks like muons, a field of  $0.1T$  allows to discriminate the charge for tracks longer than 4 meters. This corresponds for example to a muon momentum threshold of  $800 \text{ MeV}/c$ . Hence, performances are very good, even at very low momenta.

We have recently started studying the effect of the magnetic field on electrons (see Figure 3) by means of full detector simulation and reconstruction. Unlike muons or hadrons, the early showering of electrons makes their charge identification difficult. The track length usable for charge discrimination is limited to a few radiation lengths after which the showers makes the recognition of the parent electron more difficult. In practice, charge discrimination is possible for high fields:

$$x = 1X_0 \rightarrow B > 0.5T \quad (21)$$

$$x = 2X_0 \rightarrow B > 0.4T \quad (22)$$

$$x = 3X_0 \rightarrow B > 0.3T \quad (23)$$

From the simulation, we found that the determination of the charge of electrons of energy in the range between 1 and 5 GeV is feasible with good purity, provided the field has a strength in the range of 1 Tesla. Preliminary estimates show that these electrons exhibit an average curvature sufficient to have electron charge discrimination better than 1% with an efficiency of 20%. Further studies are on-going.

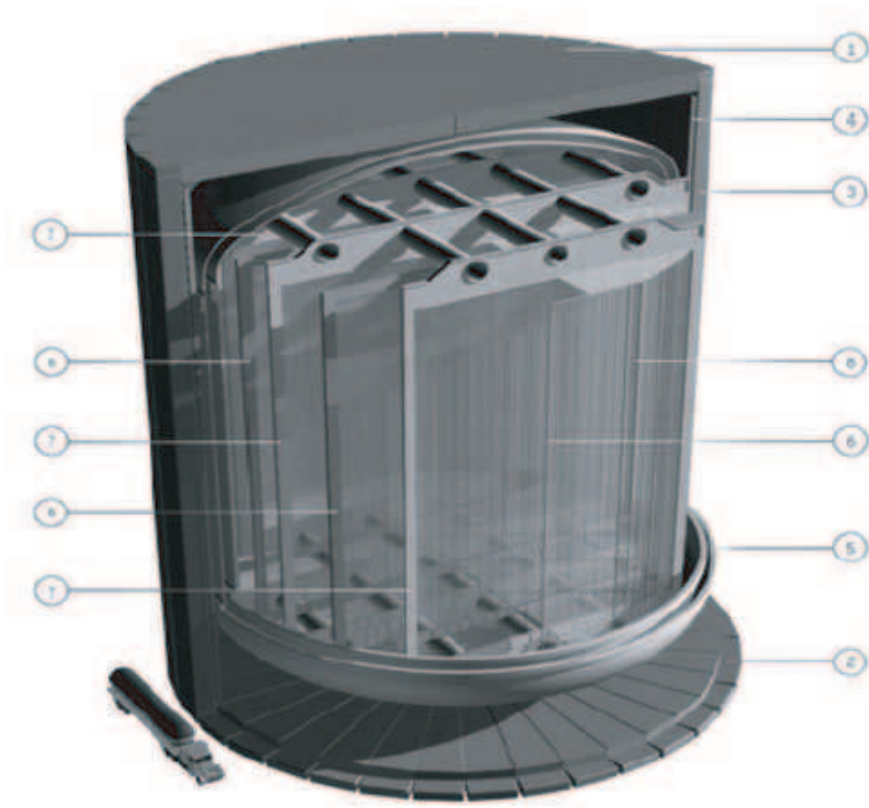


Figure 5: Artistic view of the LANNDD design[12]. See Ref. for explanation of numbers.

In parallel, we have initiated an R&D to test liquid argon imaging in a magnetic field[11] (See Figure 4). We have built a small liquid argon TPC (width 300 mm, height 150 mm, drift length 150 mm) and placed it in the recycled SINDRUM-I magnet<sup>b</sup> which allows us to test fields up to 0.5 T. The ongoing test program includes (1) checking the basic imaging in B-field (2) measuring traversing and stopping muons (3) test charge discrimination (4) check Lorentz angle. Results are expected in 2004.

The design of a magnetized liquid argon TPC of 70 kton has been considered[12]. It is based on a direct extrapolation (“scaling up”) of the technique developed by the ICARUS Collaboration, however, embedded in a very large magnet (See Figure 5). A magnetized liquid argon detector would offer unequalled physics opportunities at a neutrino factory[1, 13]. However, the technical feasibility of the enormous magnet with its gigantic yoke remains an unsolved challenge. Further engineering studies are mandatory before this technique can be proposed in an experiment of this scale.

---

<sup>b</sup>The magnet was kindly lend to us by PSI, Villigen.

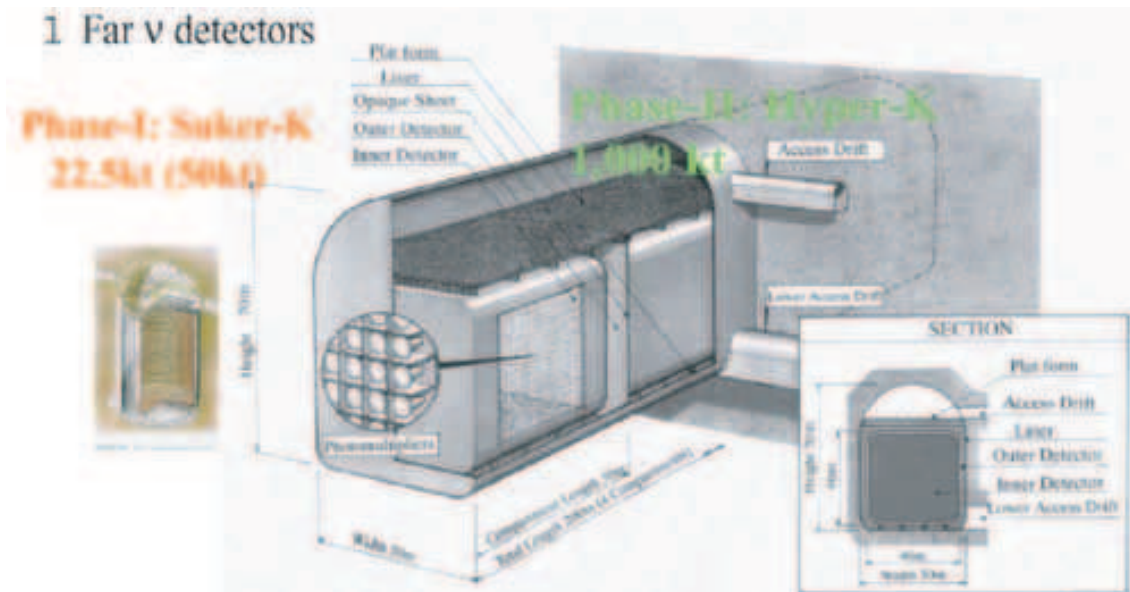


Figure 6: Super- and Hyper-Kamiokande (see Ref.[20]).

## 5 Water versus Liquid Argon

Both water Cerenkov and liquid argon detectors will cover a broad physics program, including the observation of atmospheric neutrinos, solar neutrinos, supernova neutrinos, and search for proton decays, in addition to the accelerator physics program.

Giant water detectors in the range of a megaton are perceived as a “straight-forward” extrapolation of existing detectors like SuperKamiokande[19]. There have been several proposals, as an example the design of the Hyper-Kamiokande[20] considered in the context of the JHF program is reported in Figure 6.

On the other hand, the liquid argon technique is considered as a difficult or unsafe, an almost impractical, solution for large detectors. In this section, we discuss briefly the physical properties of water and liquid argon. These are summarized in Table 1. The densities of the two liquids are very similar, with a 40% advantage for liquid Argon. The radiation and interaction lengths are rather similar, even though liquid Argon has roughly half the radiation length than water. The stopping power  $dE/dx$  of particles is similar in water and liquid Argon. Hence, neutrino interactions or other rare events will develop very similarly in liquid argon or water!

The refractive index in the visible spectrum is 1.33 for water and 1.24 for liquid Argon. This means that the Cerenkov emission properties of both media are very similar. Indeed, the Cerenkov angle  $\theta_C$  is  $42^\circ$  in water and  $36^\circ$  in liquid argon. The number of Cerenkov photons produced per track unit

Property	Water	Liquid Argon
Density ( $g/cm^3$ )	1	1.4
Radiation length (cm)	36.1	14.0
Interaction length (cm)	83.6	83.6
$dE/dx$ (MeV/cm)	1.9	2.1
Refractive index (visible)	1.33	1.24
Cerenkov angle	$42^\circ$	$36^\circ$
Cerenkov $d^2N/dEdx$ ( $eV^{-1}cm^{-1}$ )	160	130
Muon Cerenkov threshold (MeV/c)	120	140
Scintillation $\gamma/MeV$ @ $E = 0$	No	Yes, $\approx 5 \times 10^3$
Electron mobility		$500 cm^2/Vs$
Long electron drift path	no	possible

Table 1: Comparison between water and liquid Argon.

length and per unit photon energy is[14]

$$\frac{d^2N}{dEdx} = \frac{\alpha}{\hbar c} \sin^2 \theta_C \quad (24)$$

$$\approx 370 \sin^2 \theta_C \text{ eV}^{-1}cm^{-1} \quad (25)$$

Accordingly, it is  $\approx 160 \text{ eV}^{-1}cm^{-1}$  for water and  $\approx 130 \text{ eV}^{-1}cm^{-1}$  for liquid Argon. Hence, both liquids have similar Cerenkov imaging capabilities. Cerenkov light from penetrating muon tracks has been successfully detected in a liquid Argon TPC[15].

An advantage of noble liquid gases compared to water is their very high scintillation light (luminescence) yield, comparable to that of  $NaI$  crystals. The average energy needed to produce a photon is defined as  $W_\gamma$ . Its measured value (at zero electric field) is 19.5 eV for liquid Argon, 52 eV for liquid Krypton and 38 eV for liquid Xenon. This scintillation is produced[16, 17] by the de-excitation of a dimer molecule  $(Ar - Ar^+)^*$  by the emission of a single UV photon (see Figure 7). In the case of liquid Argon, scintillation appears essentially as a monochromatic line at a wavelength  $\lambda = 128 \text{ nm}$ . The produced light via this mechanism is not energetic enough to further ionize, hence, the medium is transparent to its scintillation. In addition, it should be stressed that in the liquid argon technique the medium is purified to very high levels (e.g. less than 1 in  $10^{10}$  oxygen-equivalent impurities) in order to ensure drifts of electrons over long distances without impurity attachment losses, hence it has excellent light transmission capabilities. The propagation of light is dominated by Rayleigh scattering. The scattering length is computed to be about 90 cm[18] for the scintillation line at  $\lambda \simeq 128 \text{ nm}$ . Owing to the  $\lambda^4$  dependence of the Rayleigh scattering process, we expect no effect for

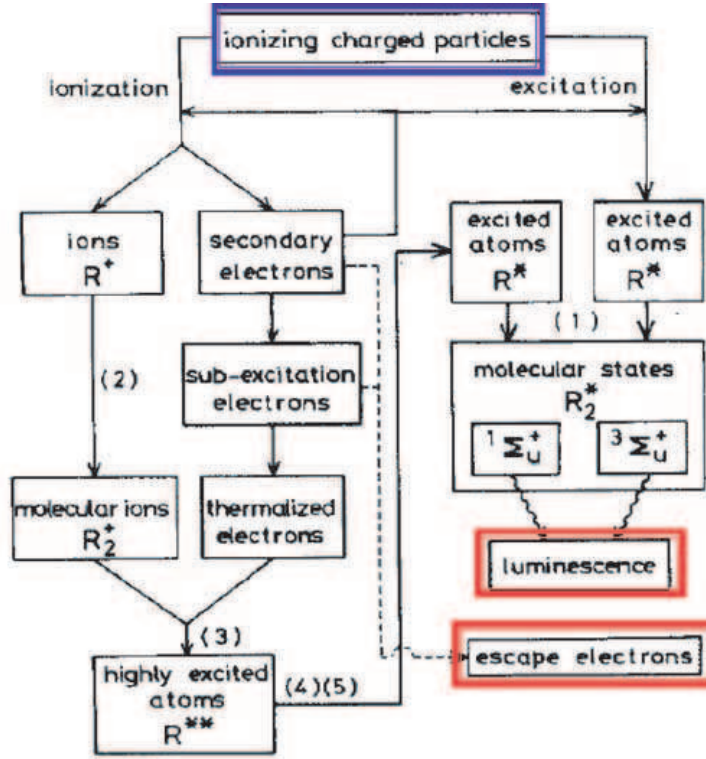


Figure 7: Processes induced by charged particles in liquid noble gases (From Ref.[17]). For particle with velocity  $\beta > 1/n$  there is also Cerenkov light emission (not included in the chart).

visible light over distances of 100's of meters. Visible photons therefore travel the medium in straight lines essentially unperturbed. It is also possible to increase the apparent scattering length of the scintillation light by doping the liquid argon with xenon (typ. 5% mixture) which shifts the light to longer wavelengths.

## 6 Combining Cerenkov, scintillation light and charge readout in a liquid Argon TPC

Since water and liquid Argon have very similar Cerenkov light emission properties and also similar physical properties in terms of radiation lengths, interaction lengths, etc.. the events in water and in liquid Argon look very much the same and the techniques developed in Kamiokande and Superkamiokande[19] for the reconstruction and analysis of events can be readily “transposed” to the liquid argon case. Hence, the performance of a liquid argon detector with Cerenkov light readout is at least equivalent to that of a giant water Cerenkov

detector from the point of view of event detection, reconstruction and analysis.

Of course, the overall performance of the liquid argon TPC profits greatly from its tracking imaging properties not available in Cerenkov imaging. The non-destructive, multiple plane readout allows to reconstruct images in space. With the imaging quality of a bubble-chamber all particles can be fully reconstructed in space, with extremely low thresholds, and the excellent calorimetry allows to reconstruct energies very precisely. Tracking and calorimetry provide momenta, particle identification, clean  $e/\pi^0$  separation, etc. Figure 8 shows for example the reconstruction of a neutral pion via Cerenkov and charge imaging. Multiple showers are difficult identify in water as their Cerenkov rings tend to easily overlap.

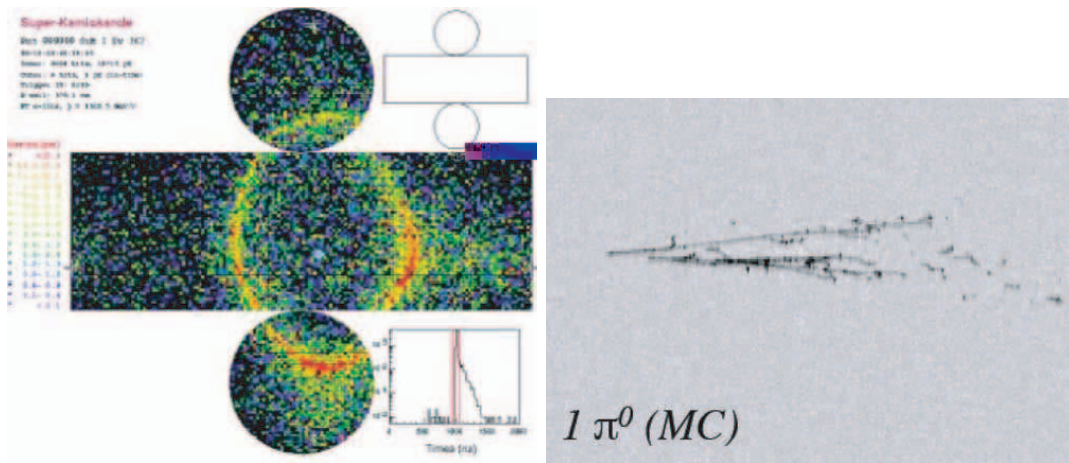


Figure 8: Neutral pion reconstruction via (a) Cerenkov (left) (b) charge imaging TPC (right) .

The most striking difference between water Cerenkov and liquid argon imaging is illustrated in Table 2, where the Cerenkov emission momentum threshold and the corresponding range in liquid argon are listed for various particles. For example, a proton becomes visible in water Cerenkov detector when its momentum is greater than 1070 MeV. At this momentum, a proton has a range of about 80 cm in liquid argon! With a typical wire pitch of 3 mm, particles like kaon, protons, etc. can be well detected down to very low momenta.

How can one then profit from the readout of the Cerenkov light in addition to the imaging? The combination of the information from the tracking, energy (e.g.  $dE/dx$  and kinetic energy) with the Cerenkov light provides improved particle identification. In particular, one can in this way separate pions from muons, a very important tool in the context beta-beams, as illustrated in Figure 9.

Particle	Cerenkov thr. in H <sub>2</sub> O (MeV/c)	Range in LAr (cm)
$e$	0.6	0.07
$\mu$	120	12
$\pi$	159	16
$K$	568	59
$p$	1070	80

Table 2: Momentum threshold for Cerenkov light emission and corresponding range in liquid Argon for various particles.

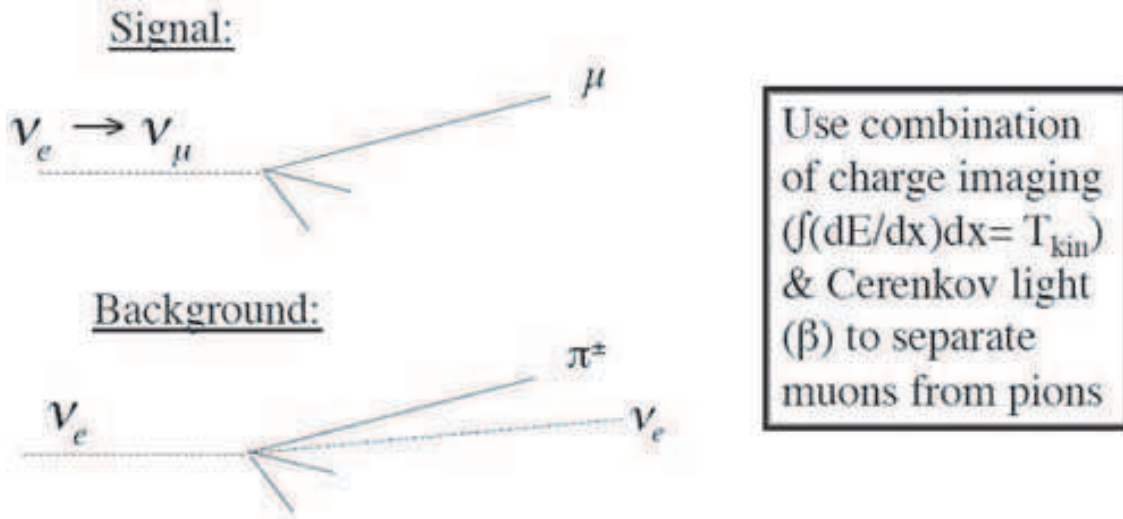


Figure 9: Illustration of signal and background given by pion/muon confusion in beta-beams, when searching for  $\nu_e \rightarrow \nu_\mu$  oscillations.

The number of photoelectrons between the wavelengths of 160 and 600 nm (the typical acceptance of a PMT) emitted by muons and pions along their trajectory before they range out is shown in Figure 10(left) as a function of the kinetic energy of the particle. We assumed a 20% coverage and a 20% quantum efficiency and that photoelectron counting is possible. In the kinetic region of interest, the number of photoelectrons varies from 1000 to 10000. Pions produce as expected slightly less photons. The statistical error is so precise that it should allow separation between the two hypotheses. For the pion, we assumed that no hadronic interaction takes place along its range. In reality, the observation of an hadronic interaction via the imaging can be used to discriminate pions versus muons. The charged pion survival probability for 90% muon acceptance efficiency is plotted in Figure 10(right). In the range between 100 MeV (threshold) and 850 MeV, the method is effective at separating muons from pions.

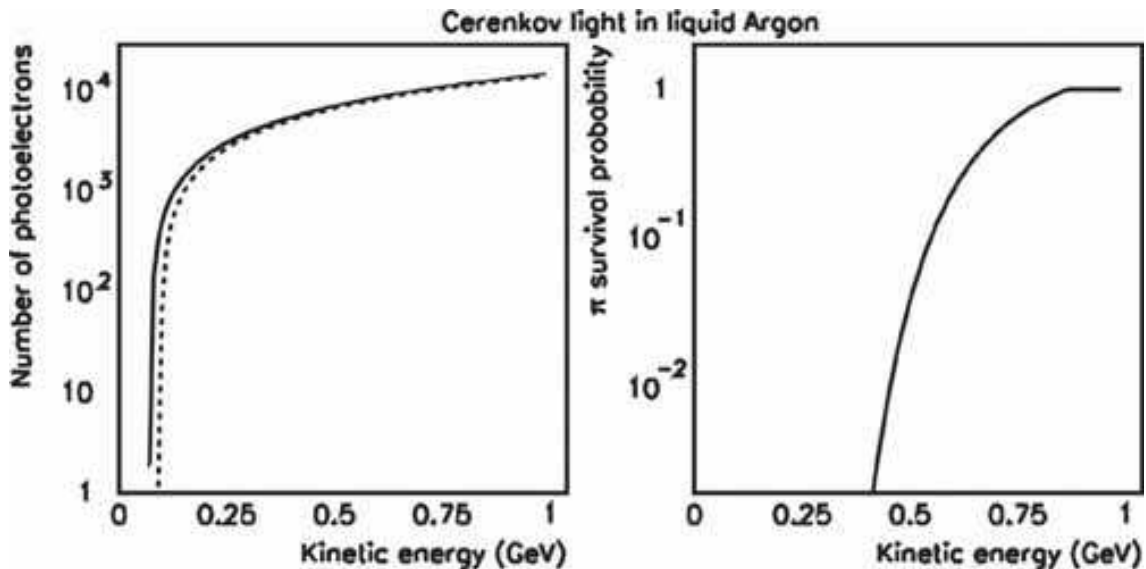


Figure 10: (Left) Number of photoelectrons between 160 and 600 nm emitted by muons (line) and pions (dashed). (Right) charged pion survival probability for 90% muon acceptance efficiency. Both quantities are plotted as a function of the kinetic energy of the particle. We assumed a 20% coverage and a 20% quantum efficiency. For the pion, we assumed that no hadronic interaction takes place along its range. In reality, the observation of an interaction via the imaging suppresses further pions versus muons.

## 7 A Giant Liquid Argon TPC with charge imaging, scintillation and Cerenkov light readout

Although the liquid argon TPC technology has been demonstrated to be mature, the possibility to construct a giant liquid argon TPC remains for many an impossible technical task. In this section, we describe some issues that to our mind show that giant liquid argon detectors might be technically feasible.

The ICARUS collaboration has proposed an underground modular T3000 detector for the LNGS laboratory based on the cloning of the T600 detector[21]. The T3000 would be composed of T600 + T1200 + T1200. The design is fully proven by the successful technical run on the surface. Further modules are ready to be built by industry. A 10 kton detector based on this design “could” be ordered today, even though this would not be most optimal financially. Following a successful scaling up strategy, one could envision building bigger supermodules based on the ICARUS-Airliquide technique, by readily increasing the dimensions of the planned ICARUS T1200 by a factor 2 in each directions: this would yield  $(2^3) \times T1200 \approx T10K$ . Hence, it seems conceivable to scale up the ICARUS dewar to a 10 kton volume. However, to reach a total mass of 100 kton would still require a large number of such supermodules (in fact,

$10 \times 10 \text{ kton} \approx 100 \text{ kton}$ , note however that the fiducial volume is less given the modularity). The modularity increases the complexity of the system.

It appears from the above discussion that contrary to a modular approach, a single giant volume is the most attractive solution. In fact, it appears that the maximum size of the single module is limited by the requirement to locate the detector underground in a cavern and not by the possibility to build a large cryogenic tanker of the needed size. Is a strong R&D program required to extrapolate the liquid Argon TPC to the 100 kton scale? Or can it be achieved in say one (or two) step(s)? In the following, we try to address the feasibility of a single volume 100 kton liquid argon detector.

## 7.1 Overview of the basic design parameters

An artistic view of the detector is shown in Figure 11. A summary of parameters are listed in Table 3. The detector can be mechanically subdivided into two parts: (1) the liquid argon tanker and (2) the inner detector instrumentation. For simplicity, we assume at this stage that the two aspects can be decoupled.

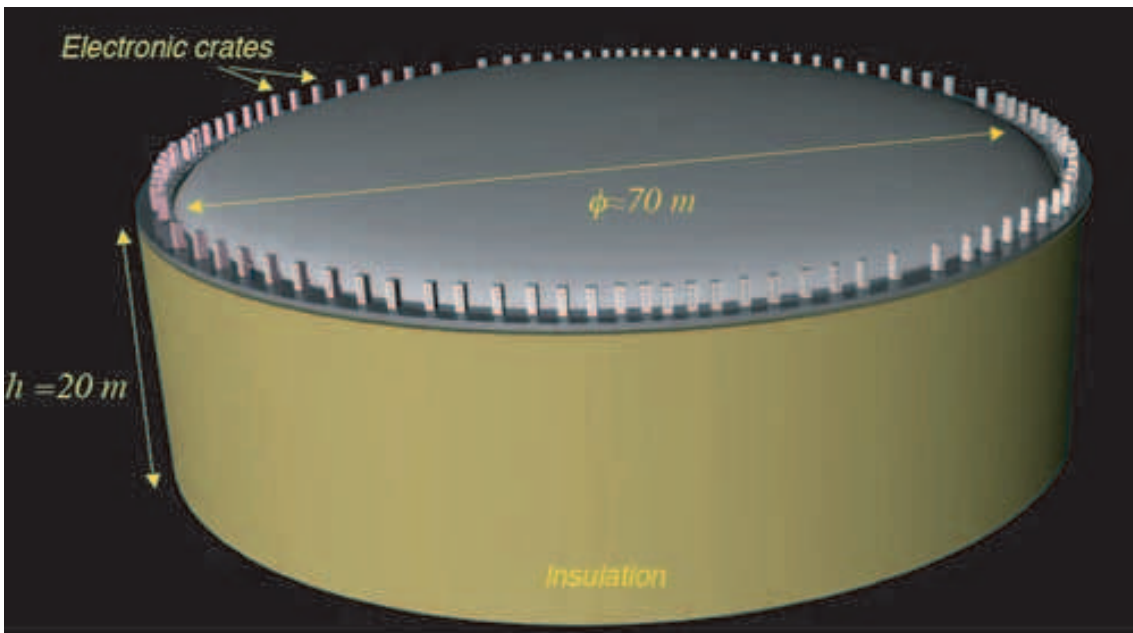


Figure 11: An artistic view of a 100 kton single tanker liquid argon detector. It appears that the feasibility of a volume of this size will be limited by the requirement to find a geologically stable underground cavern of this size. The electronic crates are located at the top of the dewar.

The basic design parameters can be summarized as follows:

1. Single 100 kton “boiling” cryogenic tanker with Argon refrigeration (in particular, the cooling is done directly with Argon, e.g. without nitrogen)
2. Charge imaging + scintillation + Cerenkov light readout for complete event information
3. Charge amplification to allow for extremely long drifts: the detector is running in bi-phase mode. In order to allow for long drift ( $\approx 20$  m), we consider charge attenuation along drift and compensate this effect with charge amplification near anodes located in gas phase.
4. Absence of magnetic field

Table 3: **Summary parameters of the 100 kton liquid Argon detector**

Dewar	$\Phi \approx 70$ m, height $\approx 20$ m, passive perlite insulated, heat input $\approx 5$ W/m <sup>2</sup>
Argon Storage	Boiling argon, low pressure ( $< 100$ mb overpressure)
Argon total volume	73118 m <sup>3</sup> (height = 19 m), ratio area/volume $\approx 15\%$
Argon total mass	<b>102365 TONS</b>
Hydrostatic pressure at bottom	$\approx 3$ atm
Inner detector dimensions	Disc $\Phi \approx 70$ m located in gas phase above liquid phase
Electron drift in liquid	20 m maximum drift, HV= 2MV for E=1 kV/cm, $v_d \approx 2$ mm/ $\mu$ s, max drift time $\approx 10$ ms
Charge readout views	2 independent perpendicular views, 3 mm pitch, in gas phase (electron extraction) with charge amplification
Charge readout channels	$\approx 100000$
Readout electronics	100 racks on top of dewar (1000 channels per crate)
Scintillation light readout	Yes (also for triggering), 1000 immersed 8”PMT with WLS (TPB)
Visible light readout	Yes (Cerenkov light), 27000 immersed 8”PMTs or 20% coverage, single photon counting capability

## 7.2 The 77’000 m<sup>3</sup> liquid argon tanker

In order to achieve such large volumes of liquid argon, we base our design on the large industrial expertise in the storage of liquefied natural gases (LNG,  $T \simeq 110K$  at 1 bar). The LNG technology has been developed quite dramatically in the last decades and was driven by the petrochemical and space rocket

industries. The technical problems associated to their design, construction and operation have already been addressed and solved by the petro-chemical industry. The current state-of-the-art contemplates tankers of  $200'000 m^3$ . Currently there seem to be in the world about 300 giant cryogenic tankers with volumes larger than  $30'000 m^3$ . Large ships transporting volumes up to  $145'000 m^3$  of LNG often cross the oceans.

LNG tanks are always of double-wall construction with efficient insulation between the walls. Large tanks are low aspect ratio (height to width) and cylindrical in design with a domed roof. Storage pressures in these tanks are very low. LNG are used when volume is an issue, in particular, for storage.

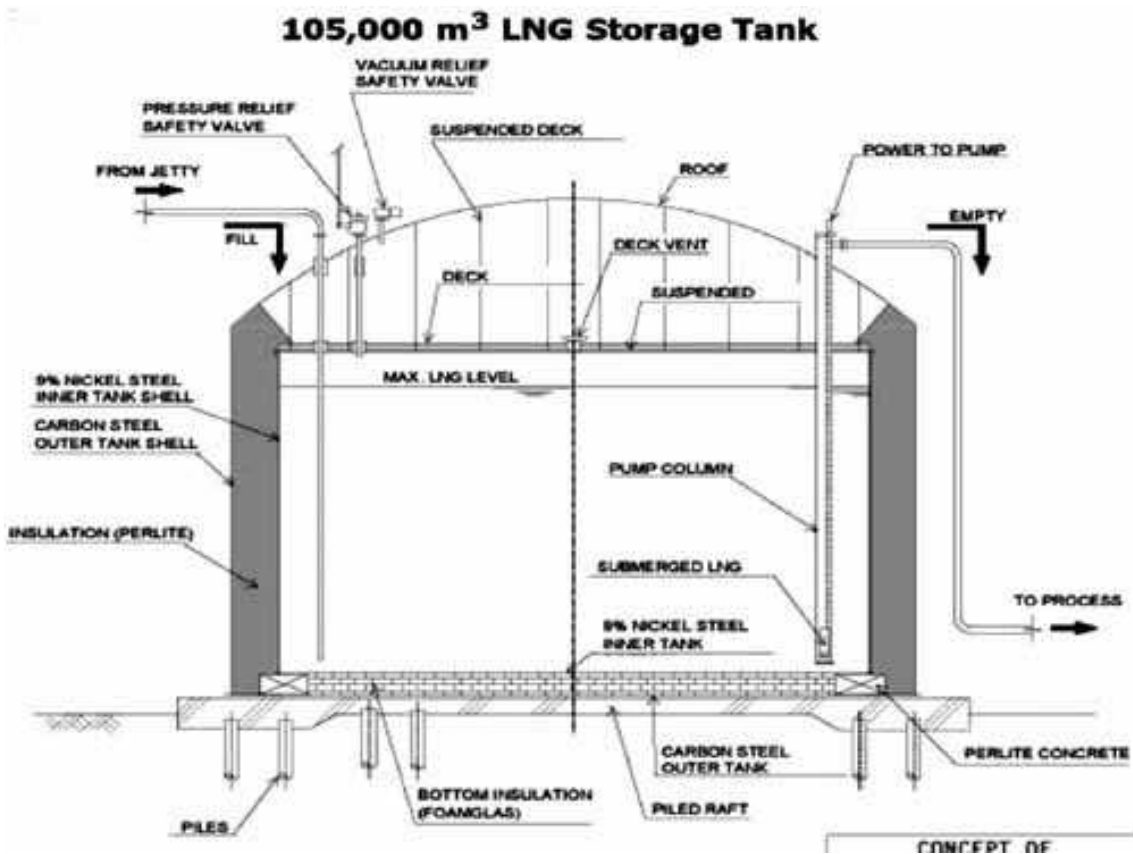


Figure 12: Engineering design of a  $105'000m^3$  cryogenic tanker developed by Technodyne International Limited (see Ref.[22]).

Of course commercial tankers are located on the surface and hence our tanker, although of reasonable size, must face the additional constraint of being located underground. We have contacted the Technodyne International Limited[22] in the UK to initiate a feasibility study in order to understand what are the issues related to the operation of a large underground liquid argon detector. Technodyne is engineering company specialized in large LNG tankers

(See Figure 12). In the baseline configuration, we are studying the design of the standard tanker (similar to those on the surface) to be located underground. The tanker will be self-supporting and will not rely on the surface of the cavern. Initial considerations seem to indicate that *the extrapolation from LNG to liquid Argon is rather straight-forward*. The geophysics of the cavern can be understood and possible movements can be predicted for periods of time extending to at least 30 years. The cooling of the cavern due to heat losses is also taken into account.

### 7.3 The inner detector instrumentation

A schematic layout of the detector is shown in Figure 13. The detector is characterized by the extremely large volume of argon. A cathode located near the bottom of the tanker is set at  $-2MV$  creating a drift electric field of  $1\text{ kV/cm}$  over the distance of  $20\text{ m}$ . In this field configuration ionization electrons are moving upwards while ions are going downward. The electric field is delimited on the sides of the tanker by a series of ring electrodes (race-tracks) put at the appropriate voltages (voltage divider). The breakdown voltage of liquid argon is such that a distance of about  $50\text{ cm}$  to the grounded tanker volume is electrically safe. For the high voltage we consider two solutions: (1) either the HV is brought inside the dewar through an appropriate custom-made HV feed-through or (2) a voltage multiplier could be installed inside the cold volume.

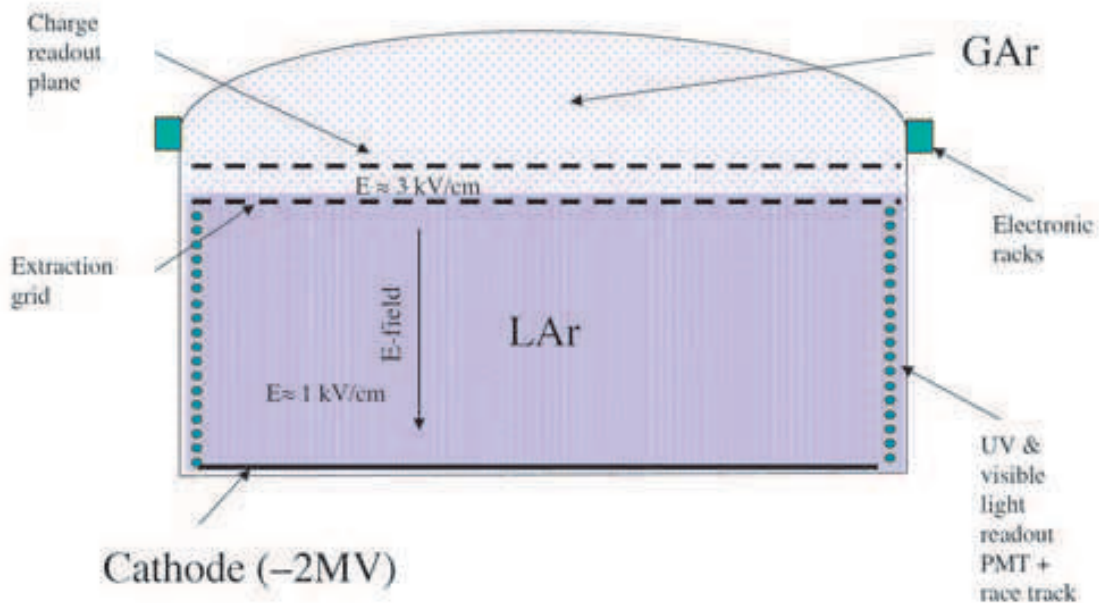


Figure 13: Schematic layout of a 100 kton liquid Argon detector.

The relevant parameters of the charge readout are summarized in Table 4. The tanker contains both liquid and gas argon phases at equilibrium. Since purity is a concern for very long drifts of the order of 20 meters, we think that the inner detector should be operated in bi-phase mode, namely drift electrons produced in the liquid phase are extracted from the liquid into the gas phase with the help of an appropriate electric field. Our measurements show that the threshold for 100% efficient extraction is about 3 kV/cm. Hence, just below and above the liquid two grids define the appropriate liquid extraction field.

Table 4: **Parameters of the charge readout**

Electron drift in liquid	20 m maximum drift, HV=2 MV for E=1kV/cm, $v_d \simeq 2\text{mm}/\mu\text{s}$ , max drift time $t_{max} \simeq 10$ ms
Charge readout views	two independent perpendicular views, 3 mm pitch
Maximum charge diffusion	$\sigma_D \simeq 2.8\text{mm}$ ( $\sqrt{2Dt_{max}}$ for $D = 4\text{cm}^2/\text{s}$ )
Maximum charge attenuation	$e^{-t_{max}/\tau} \simeq 1/150$ for $\tau = 2$ ms electron lifetime
Needed charge amplification	$10^2$ to $10^3$
Methods for amplification	Extraction to and amplification in gas phase
Possible solutions	Thin wires+pad readout, GEM, LEM, ...

In order to amplify the extracted charge, one can consider various options (1) amplification near thin readout wires (like in the MPWC, see Figure 14); (2) GEM[23] or (3) LEM[24]. Generally speaking, amplification is technically challenging since one has to operate in pure argon and one has to face problems of sparking, instabilities, etc. The addition of a quenching gas is not practical since it would pollute the liquid. It would also absorb the scintillation light from the liquid argon. Nonetheless, we have experimentally obtained encouraging results which show that a gain of 100–1000 is achievable. Since the readout is limited to the top of the detector, it is practical to route cables out from the top of the dewar where electronics crates can be located around the dewar outer edges.

Amplification operates in proportional mode. After maximum drift of 20 m at 1 KV/cm, the electron cloud diffusion reaches approximately 3 mm which is the size of the readout pitch. Hence, drifting along longer distances would start degrading the quality of the images because of the diffusion of the charge on adjacent wires. We thus think that 20 meters corresponds to a maximum conceivable drift distance. Drifting over such distances should be possible, allowing for some charge attenuation due to attachment to impurities. If we assume that the reachable electron lifetime is at least  $\tau \simeq 2$  ms (this is the value achieved on the ICARUS T600 detector during the technical run[25] and better values up to 10 ms were obtained on smaller prototypes during longer

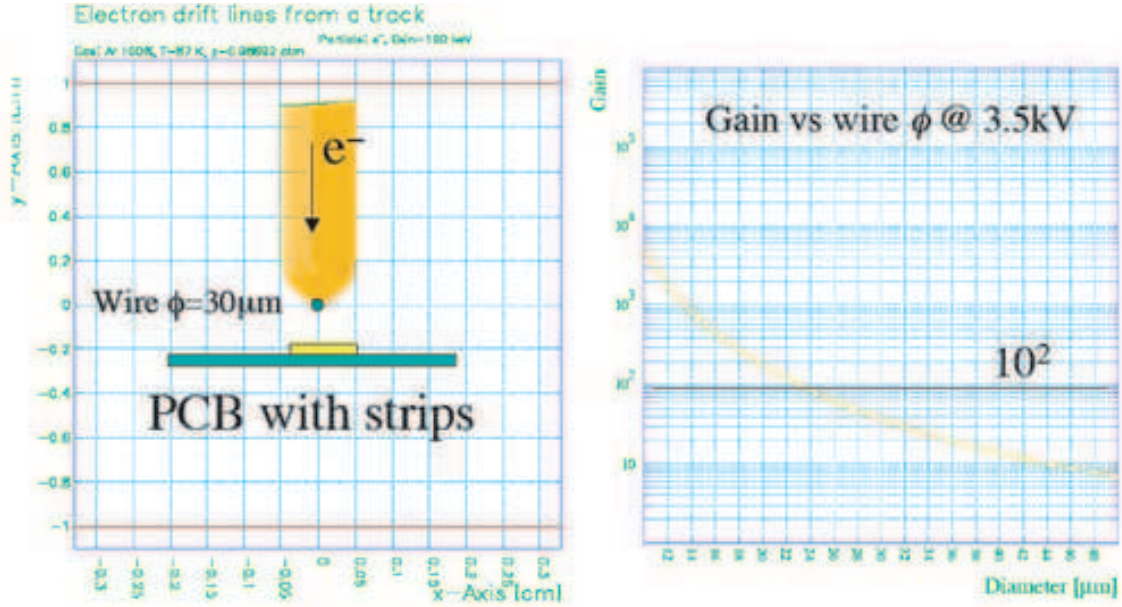


Figure 14: GARFIELD simulation for the amplification near wires in pure argon (Ar 100%,  $T=87\text{K}$ ,  $p=1\text{ atm}$ ). (left) Geometrical setup (right) gain as a function of wire diameter. The induced signals are (1) wires and (2) strips provide two perpendicular views.

runs), then we expect an attenuation of a factor  $\simeq 150$  over the distance of 20 m. This loss can be compensated by the proportional gain near the anodes.

In addition to charge readout, we envision to locate PMT's around the tanker. Scintillation and Cerenkov light can be readout essentially independently. One can profit from the ICARUS R&D which has shown that PMTs immersed directly in the liquid Argon is possible[6]. One is using commercial Electron Tubes 8" PMTs with a photocathode for cold operation and a standard glass window. In order to be sensitive to DUV scintillation, the PMT are coated with a wavelength shifter (Tetraphenyl-Butadiene).

As already mentioned, liquid Argon is a very good scintillator with about  $50000\ \gamma/\text{MeV}$ . However, this light is essentially a line at  $\lambda = 128\ \text{nm}$ . Cerenkov light from penetrating muon tracks has been successfully detected in a liquid Argon TPC[15]. This much weaker Cerenkov light (about  $700\ \gamma/\text{MeV}$  between 160 nm and 600 nm for an ultrarelativistic muon) can be separately identified with PMT's without wavelength shifter coating, since their efficiency for the DUV light will be very small.

Summarizing about 1000 immersed phototubes with WLS would be used to identify the (isotropic and bright) scintillation light. While about 27000 immersed 8"-phototubes without WLS would provide a 20% coverage of the surface of the detector. As already mentioned, these latter should have sin-

gle photon counting capabilities in order to count the number of Cerenkov photons.

## 7.4 Cryogenic aspects

In order to guarantee the safety of a tanker of this size one cannot rely on vacuum insulation. On the contrary one can use rather conventional heat insulation like for example thick layers of perlite. We envisioned an effective heat input average over the area of the detector at the level of  $5 \text{ W/m}^2$ . This is to be compared to vacuum insulations which could reach  $0.1 \text{ W/m}^2$ , however, with the risk of a vacuum loss. The tanker envisaged has a very favorable ratio of area over volume of about 15%. Hence, the heat input of 60 kW has a small effect on the big volume. See Table 5. For comparison, the refrigeration system of the CERN LHC has a cooling capacity of 140 kW at 4.5 K and CERN has since 2003 a total cryogenic capacity of 162 kW at 4.5 K.

The insulation, as efficient as it is, will not keep the temperature of LNG cold by itself. The liquid is stored as a “boiling cryogen” that is, it is a very cold liquid at its boiling point for the pressure it is being stored. The liquid will stay at near constant temperature if kept at constant pressure. This phenomenon is called “autorefrigeration”. As long as the steam (liquid vapor boil off) is allowed to leave the tank, the temperature will remain constant. Hence, the safest way to store large quantities of cryogenic liquid is at a small overpressure of less than approximately 200 mbar (basically at atmospheric pressure) and let it evaporate. While the liquid evaporates, the temperature remains constant. Since the process of evaporation is slow, the tanker remains in very stable and safe conditions.

Table 5: **Cryogenic parameters: boiling** (Heat loss should be conservative for 3 meter thick perlite and includes heat input from supports, instrumentation (cables), etc)

Dewar	$\Phi \approx 70 \text{ m}$ , height $\approx 20 \text{ m}$ , passive 3 m thick perlite insulated, assumed effective heat input $\simeq 5 \text{ W/m}^2$
Total area	$12100 \text{ m}^2$
Total heat input	60500 W
Liquid Argon evaporation rate	0.27 liters/second or 23000 liters/day
Fraction of total evaporation rate	0.03% of total argon volume per day
Time to totally empty tanker by evaporation	9 years

### 7.4.1 Initial filling

Because of the large amount liquid argon needed to fill up the experiment (e.g. 300 ton/day to fill in 300 days), we think that liquid argon could be produced locally. Other options (transport from various centers) are being investigated. If we envision a dedicated cryogenic plant, then it should be located on the surface (i.e. not underground) and connected to the detector via long vacuum-insulated pipes. See Figure 15. Hot argon gas is compressed to high pressure (typ. 200 bar) and transported towards the underground complex. In doing so, it can be purified. A heat exchanger is located before a standard Joule-Thompson expansion valve which liquifies the argon into the cryogenic tanker. The gas phase is extracted from the tanker through a heat exchanger and transported outside. Then it can either be ventilated or fed into the compressor for a further cooling cycle. This simple process is called a Linde-refrigerator.

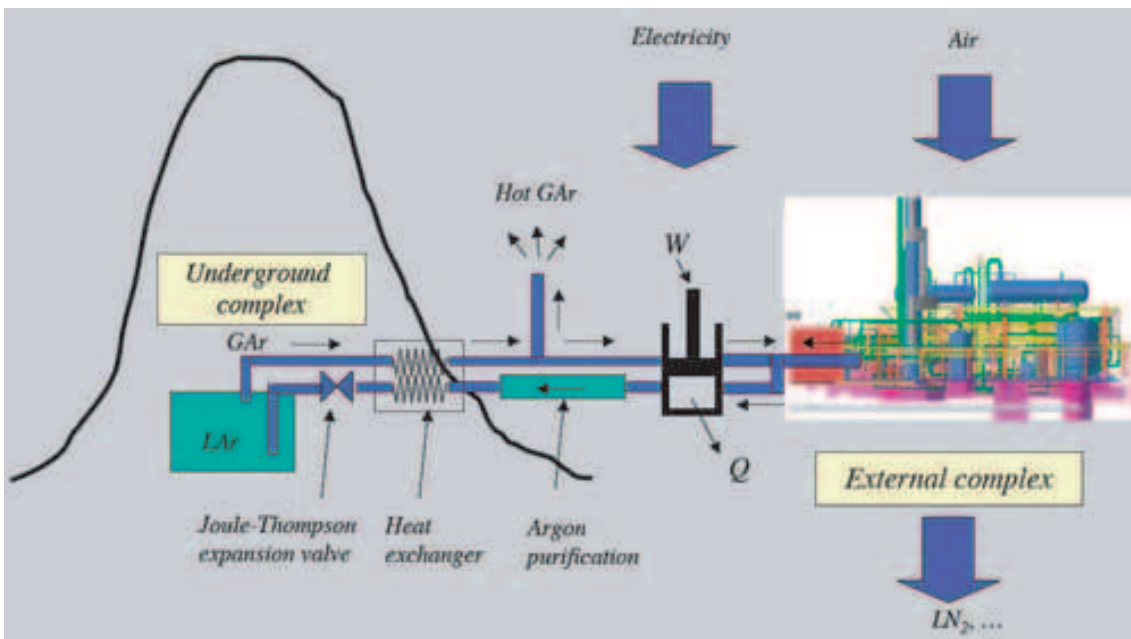


Figure 15: Cryogenic setup of the 100 kton liquid Argon detector.

The advantage of Argon is that it is naturally available everywhere in the world, since it composes approximately 1% of air (by volume air is 78,1% nitrogen, 20% oxygen, 0.93% argon, 0.033% carbon dioxide and 0.003% rare gases like neon, helium, krypton, hydrogen and xenon). Liquid Argon is hence extracted from the standard process of liquefaction from air. Air mixture is cooled down and cold gas-mixtures are separated into Oxygen, Nitrogen, Argon, ... Liquid Argon is used to fill the experiment. The rest of the gases

can be sold<sup>c</sup>. An energetically efficient method is to employ the “useless” liquids to improve the efficiency of the liquefiers.

From the energy balance point of view, the Linde-refrigerator and the process of separation of Argon from air can be ideally computed with basic thermodynamics. For a mixture of ideal gases, one has[26]

$$|W_s| = RT \sum_j y_j \ln(1/y_j) \quad (26)$$

where  $y_j$  is the mole fraction of the  $j$ th mixture. It turns out that the ideal power of separation of Argon from air is 354 kJ/kg at  $T = 300\text{ K}$ . Similarly, the ideal liquefaction process requires a work[26]

$$|W_l| = m(T(s_i - s_f) - (h_i - h_f)) \quad (27)$$

where  $s$  is the entropy and  $h$  the enthalpy of the fluid (initial, final). The ideal argon liquefaction is 478 kJ/kg at  $T = 300\text{ K}$ ,  $p = 1\text{ atm}$ . If we assume an overall thermodynamical efficiency of 5%, then we find that the total electrical power needed to fill the 100 kton tanker in two years is 30 MW. Indeed, to fill the tanker in such short time requires 150 tons of liquid argon per day! These figures are summarized in Table 6.

Table 6: **Cryogenic parameters: initial filling phase** (Initial cooling of tanker not included)

Liquid Argon 1st filling time	<b>2 years (assumed)</b>
Liquid Argon 1st filling rate	1,2 liters/second or 150 tons/day
Argon gas equivalent	85000 m <sup>3</sup> /day
Air volume equivalent (Ar 1%)	8500000 m <sup>3</sup> /day $\approx$ (205 m) <sup>3</sup> /day
Ideal power of separation of Argon mixture	600 kW (assuming for Argon 354 kJ/kg)
Ideal Argon liquefaction power	817kW (assuming for Argon 478 kJ/kg)
Assumed efficiency	5%
Estimated total plant power	<b>30 MW</b>

### 7.4.2 Operation

Even with a passive insulation, the favorable area to volume ratio of the considered tanker geometry limits the evaporation of the liquid argon to 0.03% of the volume per day. Hence, it would take 9 years to evaporate completely the tanker by evaporation (see Table 5). Once the tanker is cold and filled

---

<sup>c</sup>However, given the large quantities produced there is probably no market for it!

with argon, it will remain therefore in very stable conditions. In order not to lose mass, one must essentially “refill” the amount of liquid that is lost by evaporation. This corresponds to a loss of 0.3 liters per second. *These requirements are modest compared to those of the initial filling!* The problem lies therefore in filling the tanker in a short time and not to keep it cold. In order to produce new liquid argon (assuming the existing one is simply ventilated away, a conservative assumption), one reaches with an efficiency of 5% a power of 6.2 MW. If the liquid Argon is circulating in closed loop and we assume that the liquefaction power is still fully needed (conservative), then the power is 3.6 MW. These figures are summarized in Table 7.

Table 7: **Cryogenic parameters: refilling (refrigeration)**

Liquid Argon refilling rate	$\approx$ <b>0.3 liters/second</b> or 23000 liters/day
Argon gas equivalent	$0.2 \text{ m}^3/\text{s}$
Air volume equivalent (Ar 1%)	$20\text{m}^3/\text{s}$ or 20000 l/s
Ideal power of separation of argon mixture	130kW (assuming for Argon 354 kJ/kg)
Ideal Argon liquefaction power	180kW (assuming for Argon 478 kJ/kg)
Assumed efficiency	5%
Estimated total power	<b>6.2 MW</b>

## 7.5 Underground operation – the cavern

We believe that such a detector should be located underground in order to provide the best possible physics output given its mass. With a shallow depth, cosmic muons induced reactions which will provide dangerous backgrounds (mostly neutrons from the rock) to rare events. We are currently studying two possible configurations: (1) a cavern in a mine (with a vertical access through a shaft) (2) a cavern in a mountain (with a horizontal access through a tunnel). Work is in progress and preliminary results from these studies should be available soon.

## 7.6 Physics program

The physics program of a 100 kton target with the capability to study rare events with the quality of a bubble-chamber are vast. The physics potentialities of a giant liquid argon TPC with scintillation and Cerenkov light readout will be reported elsewhere[27]. This physics program competes favorably with a 1 Megaton water Cerenkov[20]. In terms of rates, one can mention:

- Nucleon stability: a target of 100 *kton* =  $6 \times 10^{34}$  yields a sensitivity without backgrounds of  $\tau_p/Br > 10^{34} \text{years} \times T(\text{yr}) \times \epsilon$  at the 90%C.L. This means that lifetimes in the range of  $10^{35} \text{years}$  can be reached within 10 years of operation. Channels like  $p \rightarrow \nu K$  have been shown to be essentially background free.
- Atmospheric neutrinos: about 10000 atmospheric neutrinos per year and about 100  $\nu_\tau$  charged current event per year from oscillations.
- Solar neutrinos: about 324000 events per year with electron recoil energy above 5 MeV.
- Supernova neutrinos: a SN-II explosion at 10 kpc yields about 20000 events.

In addition, one obtains 460  $\nu_\mu$  CC per  $10^{21}$  protons at 2.2 GeV (real focusing) at a distance of 130 km, and 15000  $\nu_e$  CC per  $10^{19}$   $^{18}\text{Ne}$  decays with  $\gamma = 75$  at a distance of 130 km.

## 8 Conclusions

Given the tremendous physics potential of such detectors, we invite the community to a deep reflection concerning the feasibility of giant neutrino detectors and fully compare these two options:

- Giant 1 megaton  $H_2O$  Cerenkov detector
- Giant next-generation 100 kton liquid Argon detector, taking advantages of possible advances in the LAr TPC technology like a bi-phase operation with charge amplification for long drift distances, an Imaging+Scintillation+Cerenkov readout for improved physics performance, and a Giant boiling cryostat (LNG technology)

These detectors offer the widest physics output (accelerator & non-accelerator). Coupled to the proper superbeams and beta-beams they could greatly improve our understanding of the CP-phase in the lepton sector. International sites with proper depths and infrastructure for potentially locating such giant detectors should be reviewed and compared. To build such large/giant detectors for only CP seems unconceivable, hence, giant detectors must have “broad” physics programs. Detectors should be underground (depth to be optimized vs backgrounds).

## 9 Acknowledgments

I thank Milla Baldo Ceolin for her continuous support and invitation to her series of Neutrino Telescope Workshops in the beautiful city of Venice. The

help of I. Gil-Botella and P. Sala in the physics simulation is greatly acknowledged. I thank P. Picchi, F. Pietropaolo and M. Messina for useful input, many discussions and great collaboration concerning charge extraction and amplification in essentially pure argon. The help from M. Haworth and D. Gurney from Technodyne International Limited for the conception of a giant underground liquid argon tanker is greatly acknowledged. I thank W. Pytel from the Polish CUPRUM Company for providing geophysical technical information for an underground mine location. I thank A. Zalewska for investigating mine locations in Poland. I thank L. Mosca for his time, help, and many fruitful discussions concerning the future Fréjus underground laboratory. I thank A. Bueno for useful comments on the manuscript.

## References

- [1] A. Bueno, M. Campanelli, S. Navas-Concha and A. Rubbia, Nucl. Phys. B **631** (2002) 239 [arXiv:hep-ph/0112297].
- [2] A. Rubbia, “Neutrino factories: Detector concepts for studies of CP and T violation effects in neutrino oscillations,” arXiv:hep-ph/0106088.
- [3] P. Zucchelli, *Phys. Lett.* **B532** (2002) 166.
- [4] S. Geer, Phys. Rev. D **57** (1998) 6989 [Erratum-ibid. D **59** (1999) 039903] [arXiv:hep-ph/9712290].
- [5] C. Rubbia, “The Liquid-Argon Time projection Chamber: a new concept for Neutrino Detector”, CERN-EP/77-08, (1977).
- [6] S. Amoruso *et al.*, “Design, construction and tests of the ICARUS T600 detector”, accepted for publication in Nucl. Instrum. Meth. A. and references therein.
- [7] P. Benetti *et al.*, Nucl. Instrum. Meth. A **332**, (1993) 395.
- [8] P. Cennini *et al.*, Nucl. Instrum. Meth. A **345**, (1994) 230.
- [9] F. Arneodo *et al.* [ICARUS Collaboration], *The ICARUS 50 l LAr TPC in the CERN neutrino beam*, arXiv:hep-ex/9812006.
- [10] S. Amoruso *et al.* [ICARUS Collaboration], “Measurement of the mu decay spectrum with the ICARUS liquid argon TPC,” arXiv:hep-ex/0311040. Accepted for publication in EPJ C.
- [11] M. Laffranchi, Ph.D. Dissertation, ETHZ 2004. To appear at: <http://neutrino.ethz.ch/diplomathesis.html>.
- [12] D. B. Cline, F. Sergiampietri, J. G. Learned and K. McDonald, Nucl. Instrum. Meth. A **503** (2003) 136 [arXiv:astro-ph/0105442].

- [13] A. Bueno, M. Campanelli and A. Rubbia, Nucl. Phys. B **589** (2000) 577 [arXiv:hep-ph/0005007].
- [14] K. Hagiwara *et al.*, Phys. Rev. D 66, 010001 (2002)
- [15] F. Arneodo *et al.*, [ICARUS Collaboration], *Detection Of Cerenkov Light Emission In Liquid Argon*, In press on Nucl. Instrum. Meth. A.
- [16] T. Doke *et al.*, Nucl. Instrum. Meth. A 291 (1990) 617
- [17] M. Suzuki *et al.*, Nucl. Instrum. Meth. 192 (1982) 205.
- [18] G. M. Seidel, R. E. Lanou and W. Yao, Nucl. Instrum. Meth. A **489** (2002) 189 [arXiv:hep-ex/0111054].
- [19] Y. Totsuka, Int. J. Mod. Phys. A **18S1** (2003) 273.
- [20] Y. Itow *et al.*, “The JHF-Kamioka neutrino project,” arXiv:hep-ex/0106019.
- [21] F. Arneodo et al. [ICARUS Collaboration], *Cloning of T600 modules to reach the design sensitive mass*, LNGS-EXP 13/89 add. 2/01, CERN/SPSC 2002-027 (SPSC-P-323), Nov. 2001, and references therein. Available at <http://www.cern.ch/icarus>.
- [22] Technodyne International Limited, Unit 16 Shakespeare Business Center Hathaway Close, Eastleigh, Hampshire, SO50 4SR, see <http://www.technodyne.co.uk>
- [23] F. Sauli, Nucl. Instrum. Meth. A **386** (1997) 531.
- [24] P. Jeanneret, J. Busto, J. L. Vuilleumier, A. Geiser, V. Zacek, H. Keppner and R. de Oliveira, Nucl. Instrum. Meth. A **500** (2003) 133.
- [25] S. Amoruso *et al.*, [ICARUS Collaboration], Nucl. Inst. Meth., A516 (2004) 68-79.
- [26] R.F. Barron, “Cryogenic Systems”, Oxford science publications.
- [27] I. Gil-Botella, A. Rubbia and P. Sala, in preparation and references therein.